

Safe-SAGE: Social-Semantic Adaptive Guidance for Safe Engagement through Laplace-Modulated Poisson Safety Functions

Lizhi Yang¹, Ryan M. Bena¹, Meg Wilkinson¹, Gilbert Bahati¹,
Andy Navarro Brenes², Ryan K. Cosner², Aaron D. Ames¹

Abstract—Traditional safety-critical control methods, such as control barrier functions, suffer from semantic blindness, exhibiting the same behavior around obstacles regardless of contextual significance. This limitation leads to the uniform treatment of all obstacles, despite their differing semantic meanings. We present Safe-SAGE (Social-Semantic Adaptive Guidance for Safe Engagement), a unified framework that bridges the gap between high-level semantic understanding and low-level safety-critical control through a Poisson safety function (PSF) modulated using a Laplace guidance field. Our approach perceives the environment by fusing multi-sensor point clouds with vision-based instance segmentation and persistent object tracking to maintain up-to-date semantics beyond the camera’s field of view. A multi-layer safety filter is then used to modulate system inputs to achieve safe navigation using this semantic understanding of the environment. This safety filter consists of both a model predictive control layer and a control barrier function layer. Both layers utilize the PSF and flux modulation of the guidance field to introduce varying levels of conservatism and multi-agent passing norms for different obstacles in the environment. Our framework enables legged robots to safely navigate semantically rich, dynamic environments with context-dependent safety margins.

I. INTRODUCTION

With the recent advances in bipedal and quadrupedal locomotion, the application domain for legged robots has leapt from controlled laboratory settings to semantically rich and dynamic real-world environments. As legged robots enter these human-centered domains, safety becomes paramount. While established methods such as artificial potential fields [1], model predictive control (MPC) [2], control barrier functions (CBFs) [3], and Hamilton-Jacobi (HJ) reachability [4] provide rigorous safety guarantees in the form of the forward invariance of a “safe set”, their real-world utility depends on exactly how those safe sets are constructed.

Typically, these safe sets are either “user-defined” [3], [5], learned from data [6], [7], or constructed from environmental occupancy maps and geometric primitives [8]. Such approaches are “semantically blind,” lacking a contextual understanding of the environment. For example, the safe set and avoidance behavior near a human and a chair will be identical if they occupy the same geometric volume. This indifference forces traditional controllers to either be universally conservative, which degrades performance in cluttered spaces, or universally aggressive, which risks safety failures. While some prior work introduced state-dependent

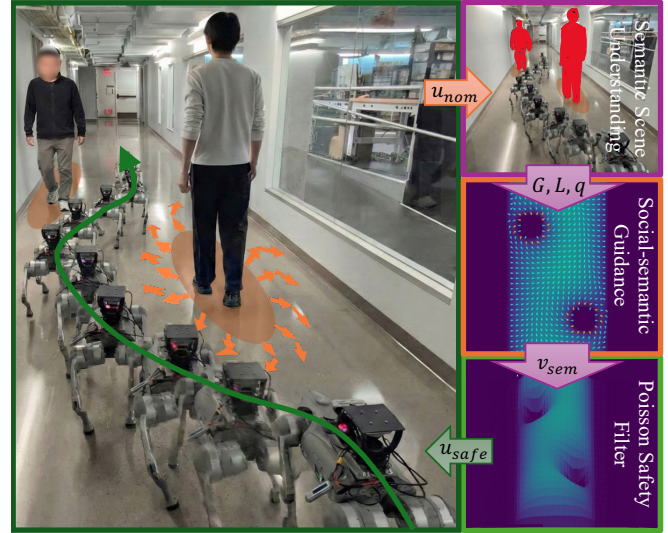


Fig. 1. Safe-SAGE in action: A quadruped robot navigates a hallway with humans moving both towards and away from it. The robot successfully avoids collisions with humans and maintains social norms, passing on the left side of the humans.

relaxations to tune conservatism [9], these methods require hand-designed relaxations that cannot autonomously incorporate environmental context.

Including semantics in the safe set synthesis process introduces new challenges, where, unlike traditional methods [3], [4], the definition of safety becomes more nuanced and extends beyond simple collision avoidance. In this case, safety becomes a context-dependent property—e.g., a hospital robot is required to distinguish between walls that permit grazes and patients that demand a wide berth. Although the recent explosion of large language models (LLMs) and vision-language models (VLMs) has enabled robots to reason about these semantics and social norms [10], [11], a critical modality mismatch prevents the direct application of these models to dynamic safety enforcement. Namely, the large models operate at low frequencies with high latency, whereas the safety filter and underlying controller operate at much higher frequencies and require near-real-time latencies.

In this paper, we propose a unified framework to bridge this *neuro-symbolic gap*. We extend the theory of Poisson safety functions (PSFs) [12] and Laplace guidance fields (LGFs) [13] to construct a semantics-aware safety layer that exists between perception and control. Our approach is distinguished by two key mechanisms: 1) we utilize semantic

All authors affiliated with Caltech MCE¹ and Tufts ME². This research is supported in part by the Technology Innovation Institute (TII), BP p.l.c., and by Dow via project #227027AW.

flux modulation to adapt safety constraint activation near obstacle boundaries, and 2) we enable social navigation by introducing a rotational component to the LGF, which encourages socially-compliant avoidance behaviors [14]. The resultant LGF guides the safe behavior of the robot with variable conservativeness. To enforce safety constraints on hardware, we implement a layered approach [15] where an MPC safety filter [16] plans optimal trajectories over a finite horizon, subject to linearized CBF constraints derived from the semantic LGF and a real-time safety filter using an analytical CBF formulation augmented σ -scaling for numerical robustness against discrete-grid artifacts. This combination ensures optimal planning behavior while guaranteeing immediate reactivity to dynamic hazards.

A. Contributions

The main contributions of this work are threefold: 1) a formulation for embedding social biases directly into the Laplace guidance field to enforce directional avoidance norms, 2) a formal analysis of the modified guidance field, and 3) a pipeline for integrating class-aware inflation and semantic flux modulation to generate obstacle-conforming safety and guidance fields from real-time perception.

B. Related Work

The synthesis of semantic reasoning with safety-critical control lies at the intersection of geometric safety and learning for semantics, utilizing Poisson safety functions.

Geometric safety focuses on the invariance of a geometric set. In general, safety-critical control methods enforce safety by constraining control inputs to render a safe set invariant [3], [5], [17]. Safety constraints that are defined based on the geometry of the robot must be converted to constraints on the system dynamics. This is achieved in MPC using the planning horizon and system dynamics model, in HJ methods by calculating the backwards reachable tube of the unsafe region [4], [18], and in CBFs by high-relative degree methods [19] or structured multi-layer constraint synthesis procedures [20]. These methods do not distinguish between objects semantically; thus, may lead to universal conservatism or unsafe aggression. Our proposed method extends geometric safety methods [12], [16] by incorporating semantic information using an onboard vision model, thus enabling the online synthesis of *context-aware* safe sets.

Safety from semantics utilizes large vision/language models for robotic safety. Language-conditioned planning [10], [21] grounds semantic instructions to robotic capabilities. Other works attempt to learn barrier functions directly from data [7], [22] or for multi-agent systems [6]. With the advancement of LLMs and VLMs, works such as [11], [23], [24] generate barrier conditions from visual-language queries. [25], [26] extend the notion of safety to hard-to-describe safety conditions by leveraging HJ reachability and latent-space safe sets. These methods operate largely at the planning layer, ensuring semantic feasibility but often fail to provide execution-level guarantees against dynamic disturbances. Our approach, through the combination of the

MPC and the real-time safety filter, safeguards the robotic system against such scenarios.

Harmonic potentials [27] guarantee local-minima-free navigation, with [28] investigating invariant sets for integrators using similar principles. More recent work [12] established the Poisson safety function framework, which utilizes as an MPC constraint [16] and [13] further expands it to support context-based risk assignment. Our work is the first to introduce semantic flux modulation into this architecture, enabling semantic-aware social and safety compliance.

Social navigation requires the robot to adhere to social norms when navigating in human environments [29]. Early works utilized the social force model [30] to simulate pedestrian dynamics. More recent approaches leverage deep reinforcement learning [31] or topological invariants [14] to learn cooperative behaviors. Gaussian processes are also used to address the “freezing robot” problem in dense crowds [32], and generative models have been used to generate socially plausible trajectories [33]. However, these methods lack the rigorous safety guarantees of CBFs or require heavy computational resources, which is not ideal for real-time operation. Our flux-modulated guidance field naturally embeds social behaviors directly into the real-time safety filter, ensuring both social compliance and rigorous safety.

II. BACKGROUND

Reduced-Order Models provide a means of representing a high-dimensional robotic system (with dynamics $\dot{\zeta} = \phi(\zeta, \mathbf{u})$, $\zeta \in \mathbb{R}^n$, and $\mathbf{u} \in \mathbb{R}^m$) as a reduced-order system by considering a reduced-order state $\mathbf{q} \in \mathbb{R}^{n_q}$, $n_q < n$, where \mathbf{q} can capture important bulk behavior such as the position of the robot centroid. Thus, given the projection $\mathbf{p} : \mathbb{R}^n \rightarrow \mathbb{R}^{n_q}$ that projects the full-order state to the reduced-order state, a feedback control law $\mathbf{u} = \mathbf{k}(\mathbf{q}) \in \mathbb{R}^{m_q}$, $\mathbf{k} : \mathbb{R}^{n_q} \rightarrow \mathbb{R}^{m_q}$, and a control interface $\kappa(\zeta, \mathbf{u})$ that lifts the reduced-order input \mathbf{u} to the full-order input \mathbf{u}_{full} , the reduced-order state \mathbf{q} satisfies the following [34], [35]:

$$\begin{aligned} \dot{\mathbf{q}} &= \frac{\partial \mathbf{p}}{\partial \zeta} \phi(\zeta, \kappa(\zeta, \mathbf{u})) \approx \mathbf{f}(\mathbf{q}) + \mathbf{g}(\mathbf{q})\mathbf{u} \\ &= \mathbf{f}(\mathbf{q}) + \mathbf{g}(\mathbf{q})\mathbf{k}(\mathbf{q}). \end{aligned} \quad (1)$$

Safety Filters enforce safety constraints on the reduced-order system, which can be characterized using a *safe set* \mathcal{C} :

$$\begin{aligned} \mathcal{C} &:= \{\mathbf{q} \in \mathbb{R}^{n_q} \mid h(\mathbf{q}) \geq 0\}, \\ \partial \mathcal{C} &:= \{\mathbf{q} \in \mathbb{R}^{n_q} \mid h(\mathbf{q}) = 0\}, \\ \text{int}(\mathcal{C}) &:= \{\mathbf{q} \in \mathbb{R}^{n_q} \mid h(\mathbf{q}) > 0\}, \end{aligned} \quad (2)$$

where the 0-superlevel set of a continuously differentiable function $h : \mathbb{R}^{n_q} \rightarrow \mathbb{R}$ represents the safe subset of the reduced-order state space, \mathbb{R}^{n_q} . Thus, the aim of a safety filter is to enforce the forward invariance of \mathcal{C} [36].

Definition 1 ([36]). A continuously differentiable function $h : \mathbb{R}^{n_q} \rightarrow \mathbb{R}$, satisfying $\nabla h(\mathbf{q}) \neq 0$ when $h(\mathbf{q}) = 0$, is a

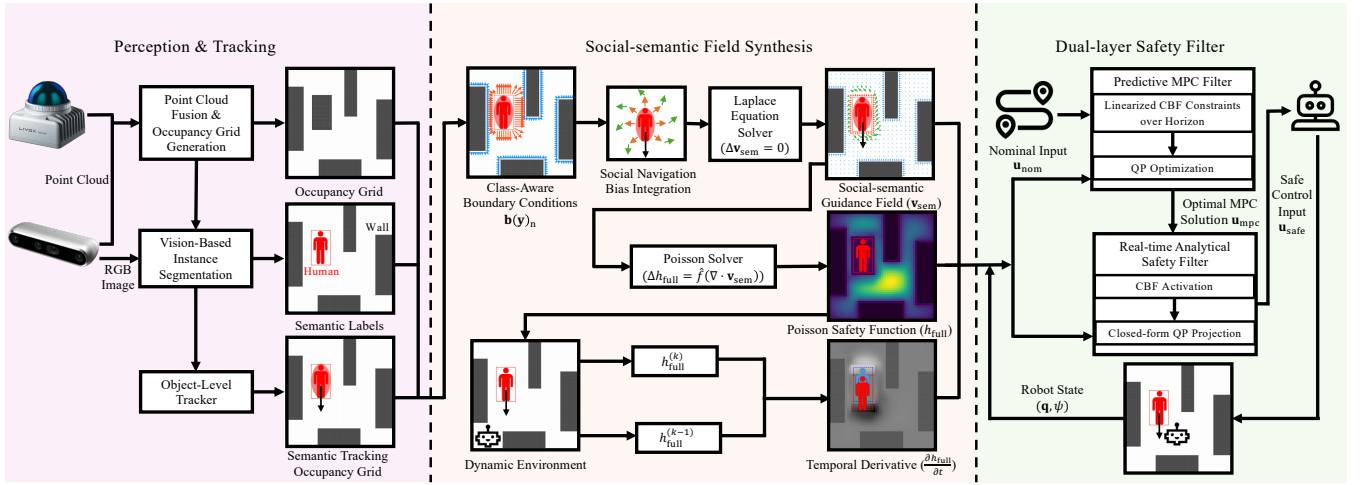


Fig. 2. System Architecture: The robot takes in multi-sensor point clouds and RGB images from the camera, performs semantic segmentation and object tracking to build a semantic occupancy grid, and then uses it to generate a social-semantic guidance field and Poisson safety function, then apply it in both real-time and predictive safety filters to ensure safety and social compliance.

control barrier function (CBF) for (1) on \mathcal{C} if there exists $\gamma \in \mathcal{K}_\infty^e$ such that for all $\mathbf{q} \in \mathbb{R}^{n_q}$, the following holds:

$$\sup_{\mathbf{u} \in \mathbb{R}^{m_q}} \left\{ \underbrace{\nabla h(\mathbf{q}) \mathbf{f}(\mathbf{q})}_{L_f h(\mathbf{q})} + \underbrace{\nabla h(\mathbf{q}) \mathbf{g}(\mathbf{q}) \mathbf{u}}_{L_g h(\mathbf{q})} \right\} \geq -\gamma(h(\mathbf{q})), \quad (3)$$

where ∇h denotes the gradient of h .

Choosing inputs \mathbf{u} that satisfy this constraint then results in system safety, i.e., the control invariance of \mathcal{C} [36, Thm. 2].

Thus, the following CBF-QP controller ensures safety by minimally modifying a nominal control action \mathbf{k}_{nom} :

$$\begin{aligned} \mathbf{k}_{safe}(\mathbf{q}) &= \underset{\mathbf{u} \in \mathbb{R}^{m_q}}{\operatorname{argmin}} \|\mathbf{u} - \mathbf{k}_{nom}(\mathbf{q})\|_2^2 \\ \text{s.t. } & L_f h(\mathbf{q}) + L_g h(\mathbf{q}) \mathbf{u} \geq -\gamma(h(\mathbf{q})). \end{aligned} \quad (4)$$

Since, in real-world robotic systems, sensors and control inputs are typically implemented with a zero-order hold, we also employ the discrete-time CBF for systems of the form:

$$\mathbf{q}_{k+1} = \mathbf{F}(\mathbf{q}_k, \mathbf{u}_k), \quad (5)$$

where the discrete-time formulation is as follows:

Definition 2 ([37]). A function $h : \mathbb{R}^{n_q} \rightarrow \mathbb{R}$ is a *discrete-time CBF* (DTCBF) for (5) on \mathcal{C} if, for some $\rho \in [0, 1]$ and each $\mathbf{q} \in \mathcal{C}$, there exists a $\mathbf{u} \in \mathbb{R}^{m_q}$ such that:

$$h(\mathbf{F}(\mathbf{q}, \mathbf{u})) \geq \rho h(\mathbf{q}), \quad (6)$$

The associated discrete-time safety filter is formulated as

$$\begin{aligned} \mathbf{k}_{safe}(\mathbf{q}) &= \underset{\mathbf{u} \in \mathbb{R}^{m_q}}{\operatorname{argmin}} \|\mathbf{u} - \mathbf{k}_{nom}(\mathbf{q})\|_2^2 \\ \text{s.t. } & h(\mathbf{F}(\mathbf{q}, \mathbf{u})) \geq \rho h(\mathbf{q}). \end{aligned} \quad (7)$$

While this may no longer be convex, [38] showed that safety can be preserved under certain convexifying approximations.

Poisson Safety Functions are a class of functions that can be used to characterize safety with respect to a spatial environment $\mathbf{q} = (x, y, z) \in \mathbb{R}^3$ [12], [13]. PSFs can

represent the safety of any environment that has a smooth, open, bounded, and connected set Ω representing the free space, with $\partial\Omega = \bigcup_{i=1}^{n_o} \partial\Gamma_i$, where $\partial\Omega$ are the surfaces of the occupied regions, Γ_i is an open, bounded, and connected set corresponding to the interior of an occupied region, and n_o is the total number of occupied regions. Given an occupancy map (numerical safe set) of the environment, we generate a PSF by solving a Dirichlet boundary value problem associated with Poisson's equation (2):

$$\begin{cases} \Delta h_0(\mathbf{q}) = \hat{f}(\mathbf{q}), & \mathbf{q} \in \Omega, \\ h_0(\mathbf{q}) = 0, & \mathbf{q} \in \partial\Omega, \end{cases} \quad (8)$$

where $\Delta = \frac{\partial}{\partial \mathbf{q}} \cdot \frac{\partial}{\partial \mathbf{q}}$ denotes the Laplacian operator, and $\hat{f} : \Omega \rightarrow \mathbb{R}_{<0}$ is a prescribed forcing term. It is noted that a smooth forcing function $\hat{f} \in C^\infty(\bar{\Omega})$ gives a smooth solution $h_0 \in C^\infty(\bar{\Omega})$ to (8) under regularity assumptions on Ω [39]. The resultant 0-superlevel set of h_0 implicitly defines a safe set \mathcal{C} such that $\Omega = \operatorname{int}(\mathcal{C})$ and $\partial\mathcal{C} = \partial\Omega$ [12]. Under suitable assumptions, the PSF is a CBF, and this constructive method enables the design of safety filters that generate admissible control inputs for systems (1) and (5).

Guidance-field-based Safety-critical Control is used to enable spatially varying conservatism around obstacle boundaries using Laplace Guidance Fields (LGFs) by explicitly prescribing safe directionality independent of the safety function's gradient. Let $\hat{\mathbf{n}}(\mathbf{q})$ be the outward unit normal for the safe set boundary at \mathbf{q} , where $b(\mathbf{q})$ is the boundary value. A guidance field $\mathbf{v} : \Omega \rightarrow \mathbb{R}^3$ satisfies the boundary flux condition

$$\mathbf{v}(\mathbf{q}) = b(\mathbf{q}) \hat{\mathbf{n}}(\mathbf{q}), \quad b(\mathbf{q}) < 0, \quad \mathbf{q} \in \partial\Omega. \quad (9)$$

We extend the field smoothly into Ω by solving the vector Laplace Dirichlet boundary value problem

$$\begin{cases} \Delta v_i(\mathbf{q}) = 0, & \mathbf{q} \in \Omega, \\ v_i(\mathbf{q}) = b(\mathbf{q}) \hat{n}_i(\mathbf{q}), & \mathbf{q} \in \partial\Omega, \end{cases} \quad i \in \{x, y, z\}, \quad (10)$$

where $v_i \in \mathbb{R}$ represents the components of \mathbf{v} .

Although \mathbf{v} is generally non-conservative and not equal to ∇h , it satisfies¹ $\mathbf{v} \parallel \hat{\mathbf{n}}$ on $\partial\Omega$. By Hopf’s Lemma [40], the outward normal satisfies² $\hat{\mathbf{n}} \propto \nabla h$ on $\partial\Omega$, enabling the generalized safety constraint

$$\mathbf{v}(\mathbf{q})^\top \mathbf{k}(\mathbf{q}) \geq -\gamma h(\mathbf{q}), \quad (11)$$

which guarantees safety for first-order systems [13, Prop. 1].

III. METHOD

In this section, we describe our social-semantic safety framework built around LGF-based PSFs. We first construct an occupancy grid with semantic labels and then use it to generate a guidance field that assigns different flux to different semantic entities and biases the field based on pre-defined social norms. Finally, we use the guidance field as the forcing function for PSF generation and apply it using both real-time and predictive safety filters. In this section, we begin with an overview of the system architecture and then detail each component: perception and tracking, field synthesis, and the dual safety filter design.

A. System Architecture

The proposed system operates as a layered safety architecture positioned between perception and control, as illustrated in Figure 2. We first fuse multi-sensor point clouds into a robot-centric occupancy grid and use a vision-based segmentation network to identify human instances. We then deploy an object-level tracker for persistent human identification outside the camera’s field of view. Finally, the resulting semantic occupancy grid feeds into a two-stage field synthesis module, where we solve Laplace’s equation with class-aware boundary conditions to construct a semantic guidance field $\mathbf{v}_{\text{sem}} : \mathbb{R}^2 \rightarrow \mathbb{R}^2$, and construct a forcing function for solving Poisson’s equation to arrive at a safety function $h_{\text{full}} : \mathbb{R}^2 \times \mathbb{S}^1 \rightarrow \mathbb{R}$. Both serve as inputs to a dual safety filter architecture operating on a reduced-order model with full state $\zeta = (\mathbf{q}, \psi)$, where $\mathbf{q} = (x, y)$ is the 2D position and ψ is the heading. The safety module consists of an analytical filter providing immediate reactive corrections and an MPC filter enforcing predictive CBF constraints. This hierarchical structure, composed of semantic perception, class-aware field synthesis, and dual-rate safety filtering, enables the system to combine the reflexive responsiveness needed for dynamic environments with the anticipatory trajectory shaping required for smooth, socially-compliant navigation, as seen in Alg. 1.

B. Semantic Environment Representation

We build a robot-centric occupancy grid by fusing point clouds from multiple sensors in the robot body frame. We mask out the robot itself using a simple hyper-elliptical filter and maintain cell occupancy using exponential decay, along with a Gaussian kernel to spatially smooth detections. An

¹ \parallel denotes that the vectors are parallel.

² \propto denotes proportionality.

Algorithm 1 Safe-SAGE

Require: Occupancy grid \mathcal{G} , class map \mathcal{L} , robot state (x, y, ψ) , nominal command \mathbf{u}_{nom}

Ensure: Safe command \mathbf{u}_{safe}

Poisson Safety Function Construction:

- 1: Extract LiDAR clusters via connected components
 - 2: Update human tracker with clusters and YOLO labels
 - 3: Label occupied cells using tracked human positions
 - 4: Compute boundary normals $\hat{\mathbf{n}}$ and class-aware flux $b(\mathbf{q})$, construct \mathbf{v}_{sem} with tangential biasing
 - 5: Solve Laplace equation $\Delta \mathbf{v}_{\text{sem}} = 0$ to construct \mathbf{v}_{sem}
 - 6: Compute forcing function $\hat{f}(\nabla \cdot \mathbf{v}_{\text{sem}})$
 - 7: Solve Poisson equation $\Delta h_{\text{full}} = \hat{f}$ for h_{full}
 - 8: Update temporal derivative $\partial h / \partial t$ via motion-compensated difference
 - 9: $\mathbf{u}_{\text{mpc}} \leftarrow$ MPC solution \mathbf{u}_0^*
 - 10: $\mathbf{u}_{\text{safe}} \leftarrow$ real-time semantics-aware safety filter (18)
 - 11: **return** \mathbf{u}_{safe}
-

instance segmentation network processes the RGB stream, provides the semantic labels, and projects them into the robot body frame to produce a sparse class map. However, this is insufficient for persistent human tracking, particularly when individuals move outside the camera’s limited field of view. To address this, we deploy an object-level tracker that associates LiDAR clusters with semantic labels over time. We first use connected component analysis [41] to extract spatial clusters from the occupancy grid and match them to existing detections via a greedy nearest-neighbor association within a tunable gating radius. The labeled clusters then update their position and velocity estimates using exponential smoothing and decay according to new detections and tracked clusters. Labeled clusters that lose association for more than the timeout threshold are pruned. The downstream safety filters can thus maintain up-to-date semantics even without fresh visual confirmation.

C. Laplace Guidance Field

To account for the robot’s orientation-dependent geometry, we parameterize the domain with the robot orientation $\psi \mapsto \Omega(\psi)$ as introduced in [16]. We construct the social-semantic guidance field $\mathbf{v}_{\text{sem}} = (v_x, v_y)$ to encode class-dependent social navigation norms by prescribing outward-normal repulsion on obstacle boundaries $\partial\Omega(\psi)$ that have class-dependent magnitude b and a tangential bias on an internal Dirichlet interface $\partial\Omega_r(\psi)$, solved via a vector Laplace equation over free space. Specifically, let $\Omega(\psi) \subset \mathbb{R}^2$ be an open, connected domain encoding free space, with a smooth boundary $\partial\Omega(\psi)$ encoding obstacle surfaces. To define $\partial\Omega_r(\psi)$, we buffer the obstacle boundaries via the Pontryagin difference [16]:

$$\bar{\Omega}_r(\psi) = \bar{\Omega}(\psi) \ominus B_r, \quad (12)$$

where $B_r = \{\mathbf{q} \in \mathbb{R}^2 \mid \|\mathbf{q}\| < r\}$ denotes the open ball of radius $r > 0$. We assume r is chosen small enough that the buffered regions surrounding distinct obstacles do not

overlap. Under the smoothness assumption on $\partial\Omega(\psi)$ and for such r , the buffered boundary $\partial\Omega_r(\psi)$ is smooth and admits well-defined outward unit normals $\hat{\mathbf{n}}_r$ and unit tangents $\hat{\tau}_r$.

On $\partial\Omega_r(\psi)$, tangential boundary conditions encode the desired social flow direction, where the sign convention on $\hat{\tau}$ determines the passing direction (e.g., pass-on-the-right). On $\partial\Omega(\psi)$, outward-normal conditions encode repulsion. Specifically, for each component $i \in \{x, y\}$:

$$\begin{cases} \Delta v_i(\mathbf{q}, \psi) = 0, & \mathbf{q} \in \Omega(\psi) \setminus \partial\Omega_r(\psi), \\ v_i(\mathbf{q}, \psi) = \lambda(\mathbf{q}, \psi) \hat{\tau}_i(\mathbf{q}, \psi), & \mathbf{q} \in \partial\Omega_r(\psi), \\ v_i(\mathbf{q}, \psi) = b(\mathbf{q}, \psi) \hat{n}_i(\mathbf{q}, \psi), & \mathbf{q} \in \partial\Omega(\psi), \end{cases} \quad (13)$$

where $\lambda(\mathbf{q}, \psi) < 0$ controls the social flow magnitude and $b(\mathbf{q}, \psi) < 0$ the repulsion magnitude. Since $\partial\Omega(\psi)$ and $\partial\Omega_r(\psi)$ are smooth and the boundary data is smooth, the Dirichlet problem is well-posed by classical elliptic theory [39]. The solution is smooth on each subdomain $\mathcal{A}_r(\psi) = \Omega_r(\psi) \setminus \bar{\Omega}(\psi)$ and $\Omega_r(\psi)$, continuous across $\partial\Omega_r(\psi)$ by construction, and Lipschitz on $\bar{\Omega}(\psi)$.

Remark 1. As established in [12], [13], Laplace guidance fields are non-conservative (i.e., they have a nonzero curl). This is the property that precisely enables the encoding of rotational social flow patterns on the closed curve $\partial\Omega_r(\psi)$.

D. Poisson Safety Function Construction

Utilizing the guidance field, we construct a scalar safety function $h_{\text{full}} : \mathbb{R}^2 \times \mathbb{S}^1 \rightarrow \mathbb{R}$ over a 3D configuration space comprising position and yaw orientation $\zeta = (\mathbf{q}, \psi)$. We can solve for the rotationally-dependent Poisson safety function:

$$\begin{cases} \Delta h_{\text{full}}(\mathbf{q}, \psi) = \hat{f}(\mathbf{q}, \psi), & \forall \mathbf{q} \in \Omega(\psi), \\ h_{\text{full}}(\mathbf{q}, \psi) = 0, & \forall \mathbf{q} \in \partial\Omega(\psi), \end{cases} \quad (14)$$

We use a smooth negative forcing function $\hat{f}(\mathbf{q}, \psi)$ following [16]. The resulting h_{full} is smooth, strictly positive in free space according to the strong maximum principle, and zero on boundaries. Importantly, the guidance field's class-aware boundary conditions propagate into the forcing function, causing h_{full} to change more quickly near semantically-critical boundaries compared to less critical obstacles.

Theorem 1 (Forward Invariance). *For a fixed ψ , consider the single-integrator system $\dot{\mathbf{q}} = \mathbf{k}(\mathbf{q})$ on $\bar{\Omega}(\psi)$ and the safe set $\mathcal{C}(\psi)$ defined as the 0-superlevel set of a continuously differentiable function $h : \bar{\Omega}(\psi) \rightarrow \mathbb{R}$. Let $\mathbf{v} : \bar{\Omega}(\psi) \rightarrow \mathbb{R}^2$ be a Lipschitz continuous vector field satisfying (13). Then for any locally Lipschitz controller $\mathbf{k} : \bar{\Omega}(\psi) \rightarrow \mathbb{R}^2$ satisfying:*

$$\mathbf{v}(\mathbf{q}) \cdot \mathbf{k}(\mathbf{q}) \geq -\gamma h_\psi(\mathbf{q}), \quad \forall \mathbf{q} \in \mathcal{C}(\psi), \quad (15)$$

for some $\gamma > 0$, the set $\mathcal{C}(\psi)$ is rendered forward invariant.

Proof. On $\partial\mathcal{C}(\psi) = \partial\Omega(\psi)$, we have $h_\psi(\mathbf{q}) = 0$, so the constraint reduces to $\mathbf{v}(\mathbf{q}) \cdot \mathbf{k}(\mathbf{q}) \geq 0$. Since $\mathbf{v}(\mathbf{q}) \parallel \nabla h_\psi(\mathbf{q})$ on $\partial\Omega(\psi)$, that is, \mathbf{v} is parallel to ∇h_ψ in the same direction, we obtain (dropping dependence on \mathbf{q} for brevity):

$$\mathbf{v} \cdot \mathbf{k} = \frac{\|\mathbf{v}\|}{\|\nabla h_\psi\|} \nabla h_\psi \cdot \mathbf{k} = \frac{\|\mathbf{v}\|}{\|\nabla h_\psi\|} \dot{h}_\psi \geq 0. \quad (16)$$

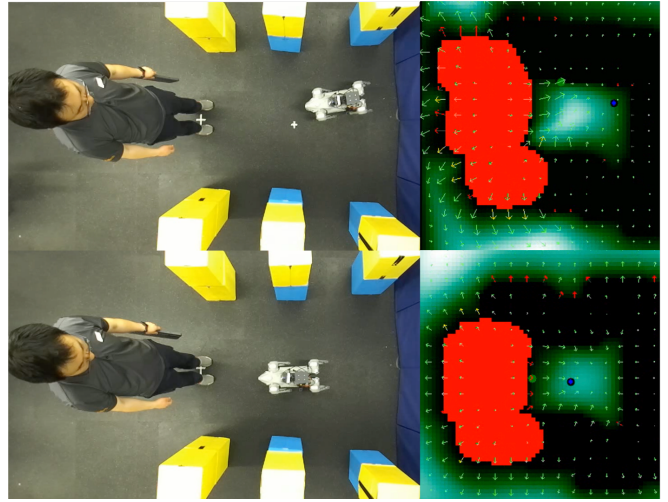


Fig. 3. An example of the biased margin induced by our proposed method. With our method enabled ($b_{\text{human}}(\mathbf{q}) = -1.7$ and $b_{\text{objects}}(\mathbf{q}) = -0.5$), the robot keeps a wider margin to the human (whose occupies states are shown in red) than the walls (in black). While without it ($b_{\text{human}}(\mathbf{q}) = -1.0$ and $b_{\text{objects}}(\mathbf{q}) = -1.0$), it keeps the same margin.

TABLE I. Safety Metrics: Human-robot margin is defined as the distance from the human to the center of the enclosed space formed by 3 walls and one human; max lateral offset is defined as the maximum distance to one side of the robot for it still to pass on other side of the human; in both larger is better.

Metric	Proposed Method	Baseline
Human-robot Margin (m)	0.318 ± 0.0774	-0.008 ± 0.0625
Max Lateral Offset (m)	0.75	-0.1

Since $\|\mathbf{v}\|/\|\nabla h_\psi\| > 0$, this implies $\dot{h}_\psi(\mathbf{q}) \geq 0$ for all $\mathbf{q} \in \partial\mathcal{C}(\psi)$. Forward invariance of $\mathcal{C}(\psi)$ then follows from Nagumo's theorem [42]. \square

E. Temporal Safety Variation

We actively estimate a temporal derivative $\partial h_{\text{full}}/\partial t$ to account for dynamic obstacles and perception latency via motion-compensated finite differences:

$$\frac{\partial h_{\text{full}}}{\partial t}(i, j, l) = \frac{h_{\text{full}}^{(k)}(i, j, l) - h_{\text{full}}^{(k-1)}(i + \delta_y, j + \delta_x, l)}{\Delta t_{\text{grid}}},$$

where (δ_x, δ_y) compensates for robot egomotion between frames and $h_{\text{full}}^{(k-1)}$ and $h_{\text{full}}^{(k)}$ are consecutive safety functions solutions separated by time Δt_{grid} . The estimate is smoothed over time using a first-order low-pass filter.

To prevent over-conservatism far from obstacles, we scale $\partial h_{\text{full}}/\partial t$ with the following σ :

$$\sigma = \min \left(\frac{\|\mathbf{v}_{\text{sem}}\|}{\|\nabla h_{\text{full}}\| + \epsilon (1 - e^{-\kappa \max(0, h_{\text{full}})})}, 1 \right). \quad (17)$$

This ensures that $\partial h_{\text{full}}/\partial t$ has its full effect near boundaries (where $h_{\text{full}} \approx 0$) but diminishes in open space.

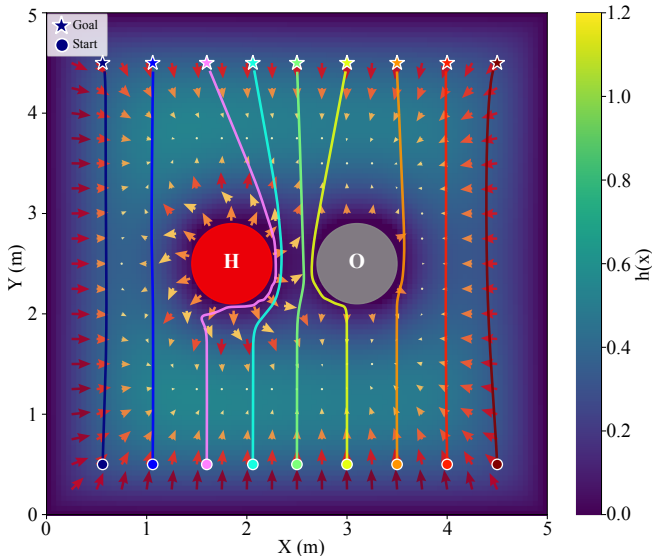


Fig. 4. Simulation benchmark of the proposed method safety filtering the robot going to the other side of the arena with a human and a static obstacle. It can be observed that the robot would exhibit social compliance unless well away from the human and also keeps a wider berth from the human than the static obstacle.

F. MPC Safety Filter

We construct an MPC optimization problem to plan safe trajectories for the future.

$$\begin{aligned}
 & \min_{\mathbf{u}_{0:N-1}} \sum_{k=0}^{N-1} (\mathbf{u}_k - \mathbf{u}_{\text{nom}})^\top P_u (\mathbf{u}_k - \mathbf{u}_{\text{nom}}) \\
 & \text{subject to } \zeta_{k+1} = \zeta_k + \Delta t \mathbf{u}_k, \\
 & \quad v_{x/y} \in [v_{x/y_{\min}}, v_{x/y_{\max}}], \\
 & \quad \omega \in [\omega_{\min}, \omega_{\max}], \\
 & \quad h_{\text{full}}(\zeta_{k+1}) \geq e^{-\gamma \Delta t} h_{\text{full}}(\zeta_k), \quad k = 0, \dots, N-1
 \end{aligned}$$

where $\zeta_k = (\mathbf{q}_k, \psi_k)$ is the full state, and the CBF constraint is evaluated using the 2D slice $h(\mathbf{q})$ at each corresponding yaw direction in lieu of the full 3D function $h_{\text{full}}(\zeta)$. We linearize the CBF constraint around the current trajectory using the guidance field \mathbf{v} for the position components and numerical differentiation for the yaw component. A Sequential Quadratic Programming (SQP) loop with line search updates the linearization point until the cost residual converges. The time-varying safety function is forward-propagated as $h_{\text{full}}(t_k) = h_{\text{full},0} + \sigma \frac{\partial h_{\text{full}}}{\partial t} t_k$ for each yaw slice, enabling proactive avoidance of closing obstacles.

G. Realtime Analytical Safety Filter

For immediate safety enforcement at the state update rate, a closed-form analytical safety filter projects the nominal velocity onto the safe control set. Given the MPC solution \mathbf{u}_{mpc} and current state $\zeta = (\mathbf{q}, \psi)$, the safety function and guidance field are evaluated via trilinear interpolation across the 3D grid. We evaluate the corresponding 2D slice

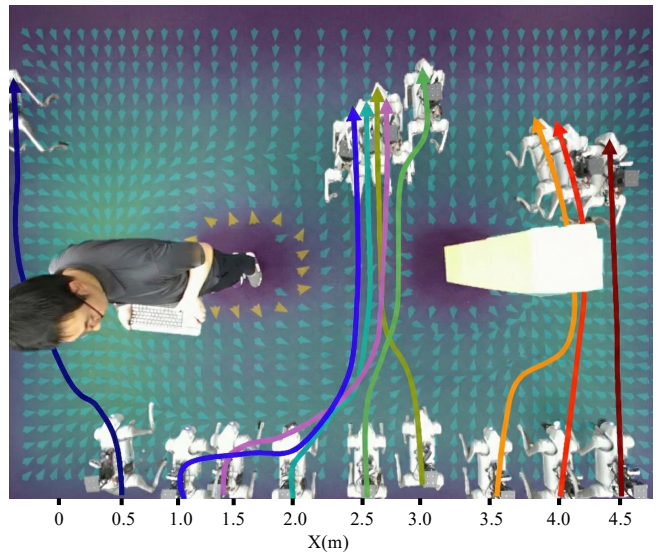


Fig. 5. Hardware experiments on the Unitree Go2 quadruped robot. Similar to the simulation benchmark, the robot is tasked with going from one side of the area to the other side. The robot behaves similarly to the simulation, keeping a wider margin to the human and observes social norms whenever possible.

$h_{\text{full}}(\mathbf{q}, \psi)$ which yields the semantics-aware safety filter:

$$\begin{aligned}
 \mathbf{u}_{\text{safe}} &= \underset{\mathbf{u} \in \mathbb{R}^3}{\text{argmin}} \|\mathbf{u} - \mathbf{u}_{\text{mpc}}\|_2^2 & (18) \\
 \text{s.t. } & \left[\mathbf{v}_{\text{sem}}(\mathbf{q}, \psi), \frac{\partial h_{\text{full}}}{\partial \psi} \right] \cdot \mathbf{u} & (19) \\
 & + \frac{\|\mathbf{v}_{\text{sem}}(\mathbf{q}, \psi)\|}{\|\nabla h\| + \sigma(h)} \cdot \frac{\partial h}{\partial t} \geq -\gamma h_{\text{full}}(\mathbf{q}, \psi).
 \end{aligned}$$

Remark 2. We note that the above semantics aware safety filter modifies $\dot{\psi}$ using $\frac{\partial h_{\text{full}}}{\partial \psi}$. Due to $\frac{\partial h_{\text{full}}}{\partial \psi}$ not being perfectly parallel to the inward pointing normal vector on the boundary of $\tilde{\Omega} = \bigcup_{\psi \in \mathbb{S}^1} \Omega(\psi) \times \{\psi\} \subset \mathbb{R}^2 \times \mathbb{S}^1$ [16], there is a discrepancy in the direction that prevents us from applying Nagumo's theorem. We can accommodate this discrepancy using a robustness term as in the ISSf-CBF literature [43]. Alternatively, we can scale the $\frac{\partial h_{\text{full}}}{\partial \psi}$ by a similar method to (17) to maintain CBF-based forward invariance guarantees.

IV. EXPERIMENTS

We quantitatively assess the effects of the social-semantic guidance field modulation on robot performance in terms of safety and social compliance, utilizing the quadruped robot Unitree Go2 for these experiments. The robot is equipped with a front UTLidar, a back mounted Livox Mid360, and a gimbal-mounted RealSense D435, as can be seen in Fig. 7. The point clouds from the three sensors are fused into a robot-centric occupancy grid. Semantic segmentation is performed by YOLOv11n, a lightweight segmentation network, which is deployed on the Jetson Orin NX onboard. The robot's odometry is estimated using FastLIO2 [44].

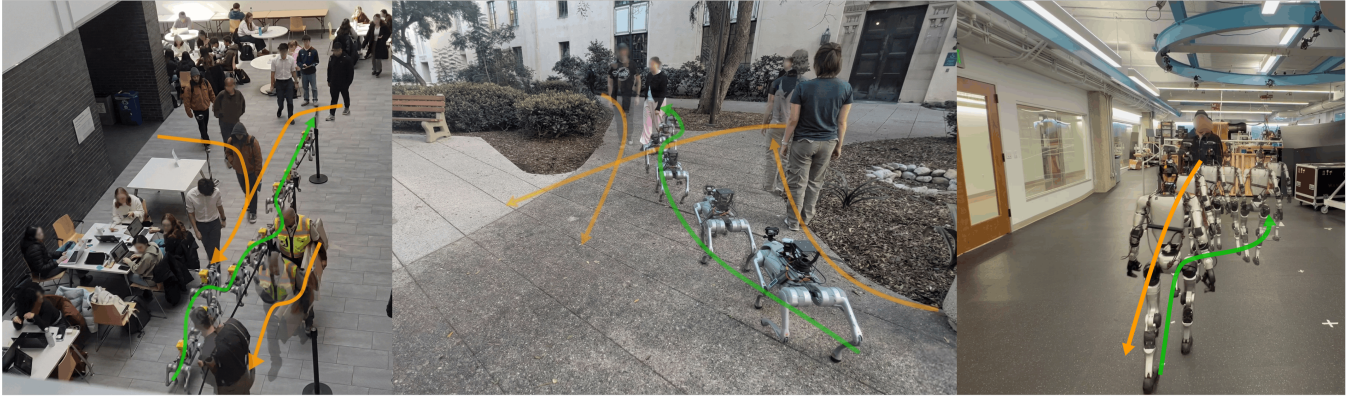


Fig. 6. Snapshots of the experiments demonstrating the effectiveness of the proposed method in different environments and on different robots. Left: Safe-SAGE deployed with different hardware setup in cafeteria; middle: Safe-SAGE deployed outside; right: Safe-SAGE deployed on a humanoid robot.

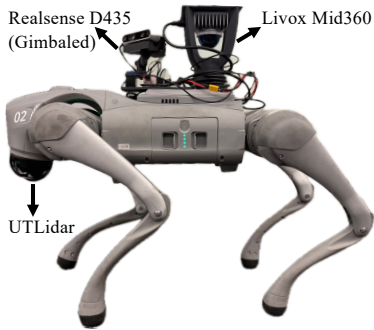


Fig. 7. The Unitree Go2 quadruped hardware setup used primarily for experiments. The point clouds from the lidars and the RGB-D camera are aggregated for occupancy map calculation, and the RGB image from the camera is used for semantic understanding.

A. Safety and Social Compliance Analysis

We construct the social-semantic compliance benchmark, requiring the robot to navigate through a gap between a human and a static obstacle, starting at different positions along the x -axis. As can be seen in Fig. 5, the behavior of the robot closely matches that of the simulation in Fig. 4.

We also perform ablation studies by comparing and quantifying our proposed guidance field modulation with the nominal guidance field, which has no importance differentiation and no tangent bias. In this case, we set up a U-shaped corridor with a human pushing the robot towards a wall. During the experiments, the human stops and the free space is enclosed, trapping the robot; thus, the safe controller is forced to stabilize in the closed safe set. We set $b_{\text{human}}(\mathbf{q}) = -1.7$ and $b_{\text{objects}}(\mathbf{q}) = -0.5$ for the proposed safety filter while setting $b_{\text{human}}(\mathbf{q}) = -1.0$ and $b_{\text{objects}}(\mathbf{q}) = -1.0$ for the nominal safety filter.

For importance differentiation comparison, we calculate the human-robot margin measured as the deviation from the center of the enclosed free space towards (negative) or away from (positive) the human; for tangent biasing effects, we find the maximum lateral offset (positive) that the robot would choose to pass on the other side of the human. As can be seen in Table I our proposed guidance field modulation achieves higher metrics in both categories.

B. Real-World Deployment Scenarios

To demonstrate the effectiveness and generalization of Safe-SAGE, we evaluate it in three scenarios as in Fig. 1 and Fig. 6: a hallway with moving pedestrians, an open area, and a crowded cafeteria. In the hallway scenario, we demonstrate the ability of our approach to successfully navigate while observing social norms with people walking towards and away from the robot. In the open area scenario, we show the robustness of our approach in handling a dynamic environment with sensory noise while maintaining safety and social compliance. In the cafeteria scenario, we validate the effectiveness and ease of use of our approach in being able to deploy to a different robot with different hardware setup (only a forward facing D435 to go with the two lidars), and its ability to maneuver around a complex environment. As our method is platform-agnostic and operates on a reduced-order model, we can deploy it on other robots with minimal modifications concerning sensor inputs and control interfaces. Thus, we are also able to deploy Safe-SAGE on the Unitree G1 humanoid robot as in Fig. 6.

V. CONCLUSION

In this paper, we propose Safe-SAGE, a unified framework that injects social-semantic awareness into robot safety filters. We extended the theory of Poisson safety functions (PSFs) [12] and Laplace guidance fields (LGFs) [13] to construct a semantics-aware safety layer that sits between perception and control, provided a formal theoretical analysis of the proposed guidance field modulation, and demonstrated its effectiveness and generalization through both simulation and hardware experiments on the Unitree Go2 quadruped robot and the Unitree G1 humanoid robot. We showed that our proposed guidance field modulation can significantly improve the robot’s ability to maintain safety and social compliance, distinguishing between semantically different obstacles and observing social norms. Looking forward, we plan to extend this framework by including better occupancy grid memory and semantic graph construction, incorporating the reasoning capability of large language models, and exploring its application in more complex social scenarios.

REFERENCES

- [1] O. Khatib, "Real-time obstacle avoidance for manipulators and mobile robots," *The international journal of robotics research*, vol. 5, no. 1, pp. 90–98, 1986.
- [2] X. Zhang, A. Liniger, and F. Borrelli, "Optimization-based collision avoidance," *IEEE Transactions on Control Systems Technology*, vol. 29, no. 3, pp. 972–983, 2020.
- [3] A. D. Ames, X. Xu, J. W. Grizzle, and P. Tabuada, "Control barrier function based quadratic programs for safety critical systems," *IEEE Transactions on Automatic Control*, vol. 62, no. 8, pp. 3861–3876, 2016.
- [4] S. L. Herbert, M. Chen, S. Han, S. Bansal, J. F. Fisac, and C. J. Tomlin, "Fastrack: A modular framework for fast and guaranteed safe motion planning," in *2017 IEEE 56th Annual Conference on Decision and Control (CDC)*, 2017, pp. 1517–1522.
- [5] S. Bansal, M. Chen, S. Herbert, and C. J. Tomlin, "Hamilton-jacobi reachability: A brief overview and recent advances," in *2017 IEEE 56th Annual Conference on Decision and Control (CDC)*, 2017, pp. 2242–2253.
- [6] Z. Qin, K. Zhang, Y. Chen, J. Chen, and C. Fan, "Learning safe multi-agent control with decentralized neural barrier certificates," *International Conference on Learning Representations*, 2021.
- [7] A. Robey, H. Hu, L. Lindemann, H. Zhang, D. V. Dimarogonas, S. Tu, and N. Matni, "Learning control barrier functions from expert demonstrations," in *2020 59th IEEE Conference on Decision and Control (CDC)*, 2020, pp. 3717–3724.
- [8] T. G. Molnar and A. D. Ames, "Composing control barrier functions for complex safety specifications," *IEEE Control Systems Letters*, vol. 7, pp. 3615–3620, 2023.
- [9] A. Alan, A. J. Taylor, C. R. He, G. Orosz, and A. D. Ames, "Safe controller synthesis with tunable input-to-state safe control barrier functions," *Control Systems Letters*, vol. 6, pp. 908–913, 2022.
- [10] M. Ahn, A. Brohan, N. Brown, Y. Chebotar, O. Cortes, B. David, C. Finn, C. Fu, K. Gopalakrishnan, K. Hausman, *et al.*, "Do as i can, not as i say: Grounding language in robotic affordances," *Conference on Robot Learning (CoRL)*, 2022.
- [11] Z. Ravichandran, D. Snyder, A. Robey, H. Hassani, V. Kumar, and G. J. Pappas, "Contextual safety reasoning and grounding for open-world robots," *arXiv preprint arXiv:2602.19983*, 2026.
- [12] G. Bahati, R. M. Bena, and A. D. Ames, "Dynamic safety in complex environments: Synthesizing safety filters with poisson's equation," *Robotics: Science and Systems (RSS)*, 2025.
- [13] G. Bahati, R. M. Bena, M. Wilkinson, P. Mestres, R. K. Cosner, and A. D. Ames, "Risk-aware safety filters with poisson safety functions and laplace guidance fields," *IEEE American Control Conference (ACC)*, 2026.
- [14] C. Mavrogiannis, P. Alves-Oliveira, W. Thomason, and R. A. Knepper, "Social momentum: Design and evaluation of a framework for socially competent robot navigation," *ACM Transactions on Human-Robot Interaction (THRI)*, vol. 11, no. 2, pp. 1–37, 2022.
- [15] E. Yamaguchi, R. M. Bena, G. Bahati, and A. D. Ames, "Layered safety: Enhancing autonomous collision avoidance via multistage cbf safety filters," *arXiv preprint arXiv:2603.00338*, 2026.
- [16] R. M. Bena, G. Bahati, B. Werner, R. K. Cosner, L. Yang, and A. D. Ames, "Geometry-aware predictive safety filters on humanoids: From poisson safety functions to cbf constrained mpc," in *2025 IEEE-RAS 24th International Conference on Humanoid Robots (Humanoids)*, IEEE, 2025, pp. 1–8.
- [17] F. Borrelli, A. Bemporad, and M. Morari, *Predictive control for linear and hybrid systems*. Cambridge University Press, 2017.
- [18] S. Bansal and C. J. Tomlin, "Deepreach: A deep learning approach to high-dimensional reachability," in *2021 IEEE International Conference on Robotics and Automation (ICRA)*. IEEE, 2021, pp. 1817–1824.
- [19] W. Xiao and C. Belta, "High-order control barrier functions," *IEEE Transactions on Automatic Control*, vol. 67, no. 7, pp. 3655–3662, 2021.
- [20] M. H. Cohen, R. K. Cosner, and A. D. Ames, "Constructive safety-critical control: Synthesizing control barrier functions for partially feedback linearizable systems," *IEEE Control Systems Letters*, vol. 8, pp. 2229–2234, 2024.
- [21] W. Huang, C. Wang, R. Zhang, Y. Li, J. Wu, and L. Fei-Fei, "Voxposer: Composable 3d value maps for robotic manipulation with language models," *arXiv preprint arXiv:2307.05973*, 2023.
- [22] K. Long, C. Qian, J. Cortés, and N. Atanasov, "Learning barrier functions with memory for robust safe navigation," *IEEE Robotics and Automation Letters*, vol. 6, no. 3, pp. 4931–4938, 2021.
- [23] L. Brunke, Y. Zhang, R. Römer, J. Naimier, N. Staykov, S. Zhou, and A. P. Schoellig, "Semantically safe robot manipulation: From semantic scene understanding to motion safeguards," *IEEE Robotics and Automation Letters*, 2025.
- [24] S. Hu, Z. Liu, S. Liu, J. Cen, Z. Meng, and X. He, "Vlsa: Vision-language-action models with plug-and-play safety constraint layer," *arXiv preprint arXiv:2512.11891*, 2025.
- [25] J. Seo, K. Nakamura, and A. Bajcsy, "Uncertainty-aware latent safety filters for avoiding out-of-distribution failures," *Conference on Robot Learning (CoRL)*, 2025.
- [26] K. Nakamura, A. L. Bishop, S. Man, A. M. Johnson, Z. Manchester, and A. Bajcsy, "How to train your latent control barrier function: Smooth safety filtering under hard-to-model constraints," *arXiv preprint arXiv:2511.18606*, 2025.
- [27] C. I. Connolly, J. B. Burns, and R. Weiss, "Path planning using laplace's equation," in *Proceedings., IEEE International Conference on Robotics and Automation*. IEEE, 1990, pp. 2102–2106.
- [28] L. Doeser, P. Nilsson, A. D. Ames, and R. M. Murray, "Invariant sets for integrators and quadrotor obstacle avoidance," in *2020 American Control Conference (ACC)*, 2020, pp. 3814–3821.
- [29] E. A. Sisbot, L. F. Marin-Urias, R. Alami, and T. Simeon, "A human aware mobile robot motion planner," *IEEE Transactions on Robotics*, vol. 23, no. 5, pp. 874–883, 2007.
- [30] D. Helbing and P. Molnár, "Social force model for pedestrian dynamics," *Physics Review E*, vol. 51, pp. 4282–4286, 1995. [Online]. Available: <https://link.aps.org/doi/10.1103/PhysRevE.51.4282>
- [31] C. Chen, Y. Liu, S. Kreiss, and A. Alahi, "Crowd-robot interaction: Crowd-aware robot navigation with attention-based deep reinforcement learning," in *2019 international conference on robotics and automation (ICRA)*. IEEE, 2019, pp. 6015–6022.
- [32] P. Trautman and A. Krause, "Unfreezing the robot: Navigation in dense, interacting crowds," in *2010 IEEE/RSJ International Conference on Intelligent Robots and Systems*. IEEE, 2010, pp. 797–803.
- [33] X. Zhou, Z. Peng, and J. Ma, "Socialtraj: Two-stage socially-aware trajectory prediction for autonomous driving via conditional diffusion model," *arXiv preprint arXiv:2509.17850*, 2025.
- [34] M. H. Cohen and C. Belta, "Safe exploration in model-based reinforcement learning using control barrier functions," *Automatica*, vol. 147, p. 110684, 2023.
- [35] M. H. Cohen, N. Csomay-Shanklin, W. D. Compton, T. G. Molnar, and A. D. Ames, "Safety-critical controller synthesis with reduced-order models," in *2025 American Control Conference (ACC)*. IEEE, 2025, pp. 5216–5221.
- [36] A. D. Ames, S. Coogan, M. Egerstedt, G. Notomista, K. Sreenath, and P. Tabuada, "Control barrier functions: theory and applications," in *2019 18th European Control Conference (ECC)*, 2019, pp. 3420–3431.
- [37] A. Agrawal and K. Sreenath, "Discrete control barrier functions for safety-critical control of discrete systems with application to bipedal robot navigation," in *Proceedings of Robotics: Science and Systems*, Cambridge, Massachusetts, 2017.
- [38] A. J. Taylor, V. D. Dorobantu, R. K. Cosner, Y. Yue, and A. D. Ames, "Safety of sampled-data systems with control barrier functions via approximate discrete time models," in *2022 IEEE 61st Conference on Decision and Control (CDC)*. IEEE, 2022, pp. 7127–7134.
- [39] D. Gilbarg, N. S. Trudinger, D. Gilbarg, and N. Trudinger, *Elliptic partial differential equations of second order*. Springer, 1977, vol. 224, no. 2.
- [40] M. H. Protter and H. F. Weinberger, *Maximum principles in differential equations*. Springer Science & Business Media, 2012.
- [41] F. Bolelli, S. Allegretti, L. Baraldi, and C. Grana, "Spaghetti labeling: Directed acyclic graphs for block-based connected components labeling," *IEEE Transactions on Image Processing*, vol. 29, pp. 1999–2012, 2019.
- [42] F. Blanchini, "Set invariance in control," *Automatica*, vol. 35, no. 11, pp. 1747–1767, 1999.
- [43] S. Kolathaya and A. D. Ames, "Input-to-state safety with control barrier functions," *IEEE Control Systems Letters*, vol. 3, no. 1, pp. 108–113, 2019.
- [44] W. Xu, Y. Cai, D. He, J. Lin, and F. Zhang, "Fast-lio2: Fast direct lidar-inertial odometry," *IEEE Transactions on Robotics*, vol. 38, no. 4, pp. 2053–2073, 2022.